ACS OMEGA

http://pubs.acs.org/journal/acsodf

Article

Reaction Mechanism of Ancestral L-Lys α-Oxidase from *Caulobacter* Species Studied by Biochemical, Structural, and Computational Analysis

Tomoharu Motoyama,[#] Yuta Yamamoto,[#] Chiharu Ishida,[#] Fumihito Hasebe, Yui Kawamura, Yasuteru Shigeta,* Sohei Ito,* and Shogo Nakano*

Cite This: *ACS Omega* 2022, 7, 44407−44419

Read Online

ACCESS | Metrics & More | Article Recommendations | Supporting Information

ABSTRACT: The flavin-dependent amine oxidase superfamily contains various L-amino acid oxidases (LAAOs) bearing different substrate specificities and enzymatic properties. LAAOs catalyze the oxidation of the α-amino group of L-amino acids (L-AAs) to produce imino acids and H_2O_2. In this study, an ancestral L-Lys α-oxidase (AncLLysO2) was designed utilizing genome-mined sequences from the *Caulobacter* species. The AncLLysO2 exhibited high specificity toward L-Lys; the k_{cat}/K_m values toward L-Lys were one and two orders larger than those of L-Arg and L-ornithine, respectively. Liquid chromatography−high resolution mass spectrometry analysis indicated that AncLLysO2 released imino acid immediately from the active site after completion of oxidation of the α-amino group. Crystal structures of the ligand-free, L-Lys- and L-Arg-bound forms of AncLLysO2 were determined at 1.4−1.6 Å resolution, indicating that the active site of AncLLysO2 kept an open state during the reaction and more likely to release products. The structures also indicated the substrate recognition mechanism of AncLLysO2; ε-amino, α-amino, and carboxyl groups of L-Lys formed interactions with Q357, A551, and R77, respectively. Biochemical and molecular dynamics simulation analysis of AncLLysO2 indicated that active site residues that indirectly interact with the substrate are also important to exhibit high activity; for example, the aromatic group of Y219 is important to ensure that the L-Lys substrate is placed in the correct position to allow the reaction to proceed efficiently. Taken together, we propose the reaction mechanism of AncLLysO2.

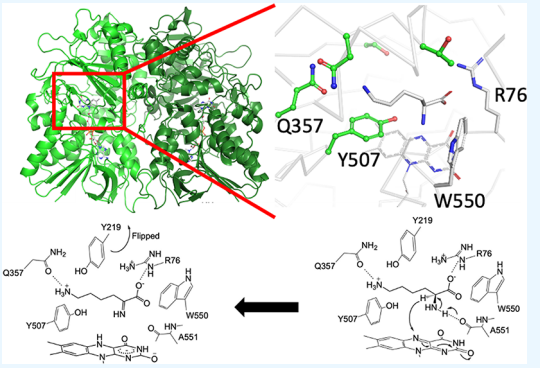

INTRODUCTION

L-Amino acids (L-AAs) are essential biomolecules not only because they are parts of proteins but also because they regulate various physiological functions. L-AA derivatives are small molecular hormones, such as epinephrine, norepinephrine, dopamine, and thyroid hormones, and the production of NO by the metabolism of L-Arg contributes to activation of the mTOR pathway.[1,2] The L-AA metabolism regulates physiological functions, and L-amino acid oxidase (LAAO) is one of the most well-known enzymes catalyzing the oxidation of the α-amino group of L-AAs to imino acid.[3,4] The products are released into the solvent and hydrolyzed to keto acids.[3,4] The reduced FAD, $FADH^-$, is reoxidized by the O_2 molecule, and H_2O_2 is generated as a second product.[4,5] LAAOs are applied to various fields, such as quantification of specific L-AAs and synthesis of fine chemicals.[3,6−9] LAAOs primarily belong to the FAD-dependent amine oxidase (FAO) superfamily, which is formed by more than 9000 non-redundant sequences; functionally uncharacterized sequences make up more than 95% of these sequences.[10]

Based on this background, we attempted to identify a new LAAO from the functionally uncharacterized sequences in the FAO superfamily, which has potential for practical application. Here, an *in silico* enzyme-screening method based on a phylogenetic approach was used to obtain novel enzymes.[11] The method adopted in this study consists of genome mining and ancestral sequence reconstruction (ASR). In the first step, a candidate for the new LAAO was assigned by paralog or homolog search with Blastp analysis. The analysis was performed by utilizing one of the functionally characterized LAAOs as a template. In the second step, ancestral enzymes of the LAAO candidates were designed by ASR. ASR is a sequence-based protein design method used to infer progenitor sequences located on each node of a phylogenetic tree utilizing multiple sequence alignments and the tree data of protein sequences.[12,13] Compared with native enzymes, the

Received: October 1, 2022
Accepted: November 9, 2022
Published: November 17, 2022

generated ancestral enzymes often exhibit outstanding properties, such as high thermal stability and productivity, without sacrificing activity.[14−16] This is a convenient way to perform the estimation of enzymatic properties by biochemical assay and structure determination using X-ray crystallography.[17] The usefulness of this method for enzyme screening is demonstrated by examples of other successful enzyme discoveries including that of a highly thermostable LAAO for stereoinversion from L-amino acids to D-form,[6] a novel proximity biotinylation enzyme named AirID,[16] and an L-glutamate decarboxylase that can be applied in gram-scale synthesis of γ-amino butyric acid from L-Glu.[18]

In the phylogenetically based screening method, success or failure is strongly dependent on which sequence is used as a template to screen enzymes. In a previous study, ancestral L-Lys α-oxidase (AncLLysO), which exhibited both oxidase and mono-oxygenase activity as well as L-Lys oxidase/monooxygenase from *Pseudomonas* AIU 813 (L-LOX/MOG),[19−21] was successfully designed by ASR using 28 sequences from *Chriseobacterium*, *Flavobacterium*, and *Pedobactor* species.[22] Blastp analysis was performed by utilizing the AncLLysO sequence as a query, indicating that many functionally uncharacterized homologs sharing moderate sequence identity (ranging from 25 to 40%) with the query were assigned. In this study, we attempted to screen new LAAO from the homologs by applying the method. After the screening of three LAAO candidates from the *Caulobacter* species was completed, their progenitor sequence was reconstructed by ASR. Enzymatic properties of the ancestral enzyme were analyzed by biochemical assay; estimation of the properties was difficult because the enzyme shared a low sequence identity with functionally characterized LAAOs, such as AncLLysO. The ancestral enzyme exhibited strong oxidase activity toward L-Lys; thus, we named this enzyme AncLLysO2. Summarizing the results of liquid chromatography−high resolution mass spectrometry (LC-HRMS), structural, and computational analysis, we attempted to clarify the unique reaction mechanism of AncLLysO2 at a molecular level compared with those already assigned to LLysOs.

MATERIALS AND METHODS

Screening and Reconstruction of Ancestral L-Lys α-Oxidase 2 (AncLLysO2). A total of three sequences (Table S1), which were annotated as "hypothetical proteins", were obtained by applying the procedure described in Figure S1. Utilizing the original Python script named "MAFFT2ASR.py" (https: //github.com/shognakano/MAFFT2ASR),[6] an ancestral sequence called AncLLysO2 was generated utilizing the obtained sequences as a template. In MAFFT2ASR.py script, the following processes were automatically performed: 1. multiple sequence alignment by MAFFT,[23] 2. generation of a phylogenetic tree by PhyML[24] with the maximum likelihood method, and 3. reconstruction of the ancestral sequence by PAML[25] utilizing the data generated. The JTT empirical models were adopted for the analysis.

Overexpression and Purification of AncLLysO2 and Their Variants. Gene synthesis service provided by Genscript was used to obtain DNA fragments encoding AncLLysO2; the his-tag is added to the C-terminal region. The purchased fragments were digested with *Nco*I and *Xho*I, and the digested fragments were subcloned into the pET28a vector, which was cut with the same two restriction enzymes. The produced expression plasmids were transformed into the *Escherichia coli* strain BL21(DE3). The cells were cultivated in 1 L of LB broth containing 30 μg/mL kanamycin at 37 °C. The temperature was lowered to 23 °C when the OD_{600} value reached 0.6−0.8, and then isopropyl-β-D-thiogalactopyranoside was added to a final concentration of 0.5 mM. Cells were harvested by centrifugation after 16 h of cultivation. The cells were suspended into buffer A (20 mM potassium phosphate [pH 7.0] and 10 mM NaCl). After sonication, the supernatant was collected by centrifugation at 11,000*g* for 40 min. The crude extract was applied to a HisTrap-HP column (GE Healthcare), and the column was washed with 30 mL of buffer A containing 5 mM imidazole. Sample solutions that contain AncLLysO2 were eluted with 15 mL of buffer A containing 20 mM imidazole. The sample solutions were applied to a MonoQ 4.6/100 PE column (GE Healthcare) that was equilibrated with buffer A and purified by applying a linear gradient obtained by mixing 10 column volume of buffer A and buffer B (20 mM potassium phosphate [pH 7.0] and 500 mM NaCl) as elution buffer. The fractions exhibiting the highest A_{450}/A_{280} ratio were collected and concentrated to 500 μL. The concentrated sample solutions were applied to a Superdex 200 Increase 10/300 GL column (GE Healthcare) equilibrated with buffer B; the purity of the samples was confirmed by SDS-PAGE. The concentration of AncLLysO2 was estimated by measuring absorbance at 280 nm; the molar extinction coefficient at 280 nm of the AncLLysO2 and the variants was calculated by Protein Calculator v3.4 (https://protcalc.sourceforge.net). The purified samples were utilized in subsequent analysis.

Site-Directed Mutagenesis of AncLLysO2. Plasmids containing AncLLysO2 cloned into pET28a were utilized as a template. Site-directed mutagenesis was performed utilizing KOD FX Neo (TOYOBO). Primers utilized to obtain the variants are listed in Table S5. Sequence confirmation of the AncLLysO2 variants was performed by DNA sequencing. The production and purification of AncLLysO2 mutants were achieved by adopting identical procedures written in the previous section. By adopting the identical calculation method indicated in a previous study,[7] FAD contents of AncLLysO2 and their mutants were estimated by measuring UV−vis absorption changes at 280 and 450 nm, indicating that the contents were distributed from 62 to 72%.

Analysis of Enzymatic Properties of AncLLysO2. The enzyme activity of AncLLysO2 was estimated by quantifying the concentration of produced H_2O_2 by the colorimetric method. By referring to a previous study,[22] the components of the reaction buffer are as follows: 10 mM L-AAs, 1.5 mM 4-aminoantipyrine, 2 mM phenol, 50 U/mL horse radish peroxidase, and 100 mM buffer. The optimal pH value was estimated by utilizing the following buffers: sodium acetate (pH 3.5−5.5), bis-tris HCl (pH 6.0−7.0), HEPES-NaOH (pH 7.5−8.0), and CAPSO (pH 9.6). Substrate selectivity was analyzed by utilizing the following buffer and substrates: 100 mM bis-tris HCl (pH 6.0) and 10 mM L-AAs. Thermostability was measured by utilizing the reaction buffer containing 10 mM L-Lys and 100 mM bis-tris HCl (pH 6.0). Prior to starting the measurement, the diluted AncLLysO2 samples were incubated for 10 min at different temperatures ranging from 30 to 80 °C. The initial velocity of AncLLysO2 was calculated by monitoring time-dependent absorption change at 505 nm with a UV−visible spectrometer (UV-2450, Shimadzu). Here, the molar extinction coefficient of the produced pigment at 505 nm was as follows: ε_{505} = 12,700 M^{-1} cm^{-1}.

https://doi.org/10.1021/acsomega.2c06334
ACS Omega 2022, 7, 44407−44419

Table 1. Enzyme Kinetic Parameters of AncLLysO2 toward the Substrates L-Lys, L-Arg, and L-Orn[a]

	AncLLysO2			AncLLysO[b]			L-LOX/MOG[c]		
substrate	k_{cat} (s^{-1})	K_m (mM)	k_{cat}/K_m (s^{-1} mM^{-1})	k_{cat} (s^{-1})	K_m (mM)	k_{cat}/K_m (s^{-1} mM^{-1})	k_{cat} (s^{-1})	K_m (mM)	k_{cat}/K_m (s^{-1} mM^{-1})
L-Lys	4.91 ± 0.08	0.086 ± 0.005	57.4	21.7	0.3	72.3	0.80	0.027	30
L-Arg	0.38 ± 0.02	1.4 ± 0.2	0.27	11.4	6.9	1.7	0.41	0.048	8.5
L-Orn	0.19 ± 0.01	33.5 ± 4.0	0.006	46.4	45.8	1.0	1.5	0.022	68

[a]The measurement of enzyme kinetic parameters was performed independently six times ($N = 6$). [b]Enzyme kinetic parameters were cited from ref 22. [c]Enzyme kinetic parameters were cited from ref 20.

Table 2. Statistics of X-ray Diffraction Data Collection of AncLLysO2 for Ligand-Free, L-Lys-, and L-Arg- Bound Form

	ligand-free	iodide-SAD	L-Lys bound	L-Arg bound
space group	$P2_1$	$P2_1$	$P2_1$	$P2_1$
unit cell parameters				
a (Å)	79.2	82.7	79.4	79.3
b (Å)	76.5	78.7	77.4	77.2
c (Å)	92.7	97.4	93.4	93.3
α (°)	90.0	90.0	90.0	90.0
β (°)	104.4	108.0	104.4	104.3
γ (°)	90.0	90.0	90.0	90.0
X-ray source	PF BL-5A	PF BL-5A	PF BL-5A	PF BL-5A
wavelength (Å)	1.00	1.70	1.00	1.00
resolution (Å)	44.9−1.55 (1.63−1.55)	46.7−2.00 (2.10−2.00)	45.3−1.40 (1.47−1.40)	45.2−1.60 (1.64−1.60)
no. of reflections[a]	1,032,997	2,069,248	1,381,298	929,719
no. of unique reflections	155,511	81,007	215,621	140,292
completeness (%)	99.8 (98.9)	98.8 (91.9)	99.1 (93.9)	98.1 (91.2)
I/sig(I)	12.6 (3.4)	51.6 (7.0)	27.2 (3.4)	26.6 (4.2)
R_{merge}[b]	0.073 (0.383)	0.046 (0.474)	0.035 (0.398)	0.043 (0.383)
$CC_{1/2}$	0.998 (0.952)	1.00 (0.983)	1.00 (0.939)	1.00 (0.934)
B of Wilson plot (Å^2)	17.09	27.4	14.95	17.24
iodide sites		68		
FOM before DM[c]		0.34		
FOM after DM[c]		0.82		
R[d]	0.163		0.158	0.152
R_{free}[e]	0.191		0.183	0.186
RMSD of geometry				
bond length (Å)	0.013		0.014	0.013
bond angles (deg)	1.78		1.87	1.74
geometry				
Ramachandran outlier (%)	0.26		0.43	0.26
Ramachandran favored (%)	97.3		97.6	98.2
Average B factor (Å^2)	20.92		18.10	20.34
protein atoms	19.4		16.18	18.66
ligand atoms	14.8		12.89	15.12
solvent atoms	31.5		29.12	30.60
PDB entry	7X7I		7X7J	7X7K

[a]The sigma cutoff was set to none ($F > 0\sigma F$). [b]$R_{merge} = \Sigma_h \Sigma_i |I_i(h) - \langle I(h)\rangle| / \Sigma_h I(h)$, where $I_i(h)$ is the ith measurement of reflection h and $\langle I(h)\rangle$ is the mean value of the symmetry-related reflection intensities. Values in brackets are for the shell of the highest resolution. [c]FOM before/after DM means the figure of merit before/after density modification. [d]$R = \Sigma||F_o| - |F_c|| / \Sigma|F_o|$, where F_o and F_c are the observed and calculated structure factors used in the refinement, respectively. [e]R_{free} is the R-factor calculated using 5% of the reflections chosen at random and omitted from the refinement.

The steady-state kinetic parameters of AncLLysO2 were estimated utilizing L-Lys, L-Arg, and L-ornithine (L-Orn) as substrates. Here, the concentration of the substrates was set as follows: 0.05−1.0 mM L-Lys, 0.5−10 mM L-Arg, and 5.0−50 mM L-Orn. pH values of the substrates were prepared to be 7.0 by adding diluted HCl solution. The enzyme kinetic parameters were estimated by fitting the initial velocity to the Michaelis−Menten equation with the non-linear least square method. The fitting was performed by Origin software, and the calculated parameters are reported in Table 1. Estimation of the enzyme kinetic parameters for AncLLysO2 variants was performed by adopting identical procedures. All experiments were performed in six replicates ($N = 6$), two biological replicates per three technical replicates.

Analysis of Products by LC-HRMS. LC-HRMS analysis was performed using maXis plus (Bruker Daltonics, Bremen, Germany). Here, the following columns were utilized to detect the products ((i) L-Lys, 5-APNA, and 5-APNM; (ii) TPCA) by LC-HRMS: (i) a UPLC column (XBridge BEH Amide XP column [length, 2.1 × 50 mm^2; inner diameter (i.d.), 2.5 μm;

https://doi.org/10.1021/acsomega.2c06334
ACS Omega 2022, 7, 44407−44419

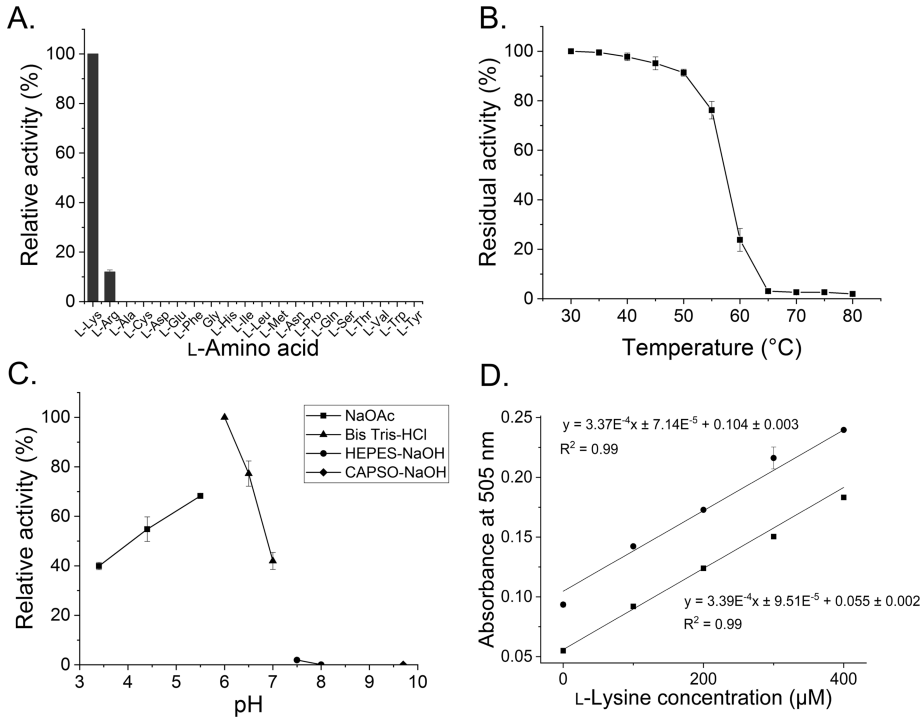

Figure 1. Biochemical analysis of AncLLysO2. Relative specific activity of AncLLysO2 toward 20 L-AAs (10 mM) (A). The enzyme exhibited the highest activity toward L-Lys. Analysis of thermostability (B) and optimal pH (C). Quantification of L-Lys by AncLLysO2 (D). Samples that contain only buffer (filled square) and human plasma (filled circle) were represented. All experiments were performed using six replicates; the average and standard deviation values were represented in the figures.

Nihon Waters K.K., Tokyo, Japan]) equipped with a guard column (XBridge BEH Amide XP VanGuard cartridge [length, 2.1 × 5 mm^2; i.d., 2.5 μm; Nihon Waters K.K., Tokyo, Japan]) and (ii) a UPLC column (XBridge Premier BEH C18 column [length, 2.1 × 50 mm^2; inner diameter (i.d.), 2.5 μm; Nihon Waters K.K., Tokyo, Japan]) equipped with a guard column (XBridge Premier BEH C18 VanGuard cartridge [length, 2.1 × 5 mm^2; i.d., 2.5 μm; Nihon Waters K.K., Tokyo, Japan]). The columns were kept at 40 °C. The volume of injected samples was 1 μL. The following two solutions were utilized as the mobile phase: (i) 0.5 mM ammonium formate and 90% (v/v) acetonitrile (solution A1) and 0.5 mM ammonium formate and 50% (v/v) acetonitrile (solution B1) and (ii) 0.1% (v/v) formic acid (solution A2) and 0.1% (v/v) formic acid in acetonitrile (solution B2). The flow rate was set to 0.3 mL/min, and the products were eluted by applying the following conditions: (i) (1) 0% B1 for 1 min, (2) 0−100% B1 over 7 min, (3) 100% B1 for 3 min, and (4) 0% B1 for 7 min and (ii) (1) 10% B2 for 1 min, (2) 10−90% B2 over 7 min, (3) 90% B2 for 3 min, and (4) 10% B2 for 7 min.

Crystallization and Structure Determination of AncLLysO2. The purified AncLLysO2 was concentrated to approximately 26 mg/mL by a centrifugal filter unit, Amicon ultra-15 centrifugal filter 10 kDa MWCO (Millipore). Crystallization of AncLLysO2 for phase determination was performed as follows. After mixing 1.5 μL of the concentrated AncLLysO2 samples with 1.5 μL of reservoir solution, composed of 0.2 M magnesium chloride hexahydrate, 0.1 M HEPES-NaOH (pH 7.5), 25% (w/v) PEG3350, and 0.1 M NDSB-256, AncLLysO2 crystals appeared at 22 °C. The crystals were soaked in a cryo-protectant for 3 h (0.1 M HEPES-NaOH [pH 7.5], 25% [w/v] PEG3350, 0.1 M NDSB-256, 20% [v/v] glycerol, and 0.1 M NaI), and the crystals were flash-cooled under a liquid nitrogen stream (100 K). X-ray diffraction data were collected using a Pilatus3 detector instrument at the BL5A beamline in the Photon Factory (Tsukuba, Japan). Integration and scaling of the data were performed by XDS[26] and SCALA,[27] respectively. The initial phase determination was achieved by the iodide single anomalous dispersion method. AutoSol, implemented in PHENIX software,[28] assigned a total of 68 anomalous sites by analyzing the data. Model building was performed by AutoBuild[28] and Coot,[29] and the initial structure for the ligand-free form of AncLLysO2 was obtained.

Structures of the L-Lys- and L-Arg-bound forms of AncLLysO2 were obtained by the following procedures utilizing the AncLLysO2 as a sample. Complexes with L-Lys or L-Arg were prepared by soaking AncLLysO2 (ligand-free form) crystals within 30 s in a cryo-protectant containing 100 mM L-Lys and 100 mM L-Arg, respectively. The soaked crystals were flash-cooled under a cryo-nitrogen stream (100 K). X-ray diffraction data were collected at BL5A in the Photon Factory. Data integration and scaling were performed by XDS[26] and SCALA,[27] respectively, and the phase was determined by the MOLREP software[30] utilizing the structure of the ligand-free form of AncLLysO2 as a template. Model building and refinement were performed by Coot[29] and either REFMAC[31] or PHENIX,[28] respectively. All figures were prepared by PyMOL.[32] Crystallographic parameters are shown in Table 2.

Molecular Dynamics (MD) Simulation. The crystal structure of AncLLysO2 (PDB ID: 7X7J) was used as the initial template. The structure of the AncLLysO2(Y219A) variant was modeled by using the structure and the Mutagenesis utility of PyMOL.[32] Hydrogen bond assignment was done at pH 7.0 using PROPKA.[33] The constructed structures were subjected to MD simulations up to 200 ns to

https://doi.org/10.1021/acsomega.2c06334
ACS Omega 2022, 7, 44407−44419

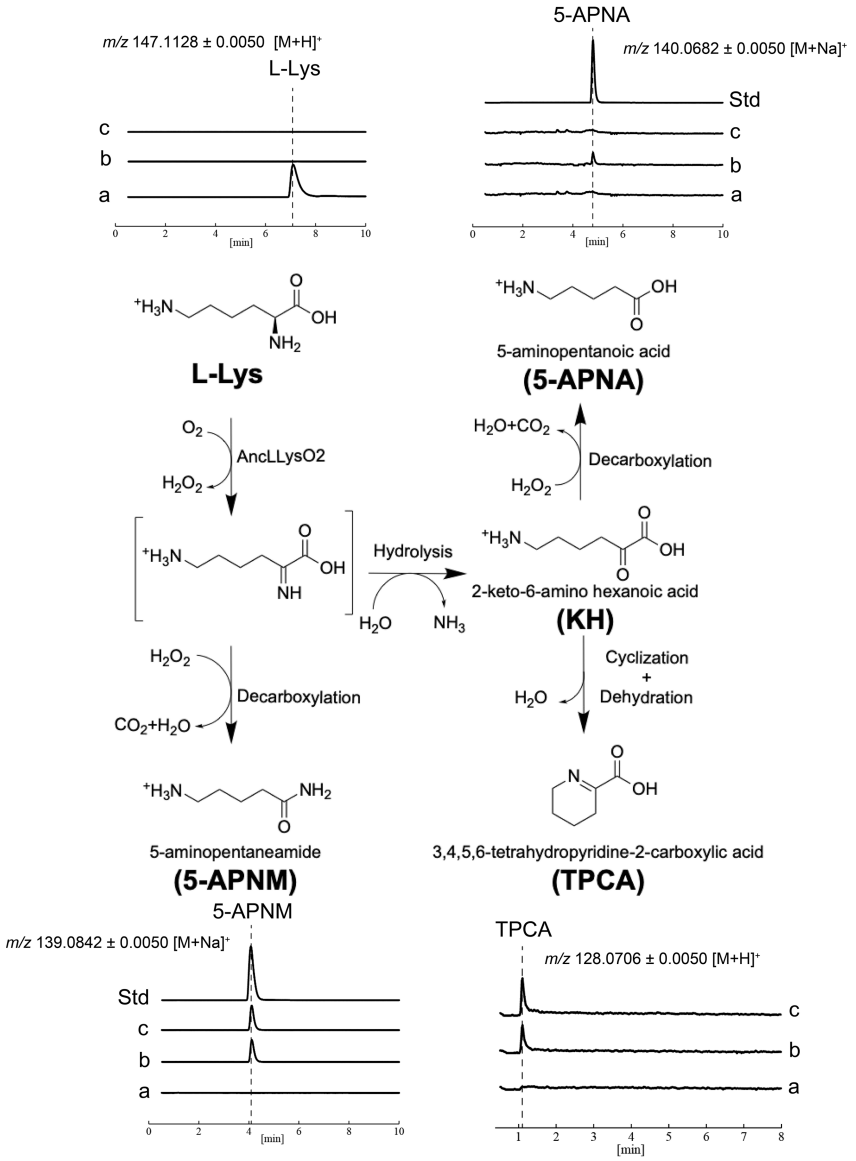

Figure 2. Assignment of reaction products of AncLLysO2 by LC-HRMS analysis. Extracted ion counts chromatograms of $[M + H]^+$ for L-Lys and TPCA, and $[M + Na]^+$ for 5-APNM and 5-APNA are represented. Each chromatogram (a−c) was obtained by measuring the samples obtained after 24 h of reaction under the following condition: a. 10 mM L-Lys, b. 10 mM L-Lys and 0.5 mg AncLLysO2, and c. 10 mM L-Lys, 0.5 mg AncLLysO2, and 1000 U catalase, respectively.

compare the dynamics of AncLLysO2 and the Y219A variant. The MD simulations were performed with explicit solvent water molecules. The simulation was performed on the system containing a total of 33,589 water molecules in the cuboid box. The size of the box was as follows: x = 119.635 Å, y = 117.215 Å, and z = 99.880 Å, respectively. For all the MD simulations, the GROMACS package[34] was used with the AMBER ff14SB force field[35] for the protein, AMBER parameter database[36] for $FADH^-$, and the TIP3P water model for the solvent. Calculations were run at 300 K and a pressure of 1 bar with the NPT ensemble.

The binding free energies were calculated using the molecular mechanics-generalized Born surface area (MM-GB/SA) approach[37] implemented in AMBER16.[38] A total of 100 conformations were extracted from the last 100 ns of the MD simulations.

RESULTS AND DISCUSSION

Genome Mining and Sequence Design of AncLLysO2.

Recently, LAAOs have been cloned from several marine bacteria.[7,39] Highly active LAAOs that can be expressed in *E. coli* have been reported by ancestral reconstructions using LAAO genes from the bacteria.[39] Based on this background, genome mining was performed to screen new LAAOs as shown in Figure S1. First, the selection of a target protein was performed by a sequence similarity search; in the sequences obtained by submitting the AncLLysO sequence to Blastp, a hypothetical protein from *Caulobacter radices* (CyHyp, WP_116490310.1) was selected as the target protein. CyHyp shared moderate sequence identity (approximately 30%) with AncLLysO, and we expected that the protein may exhibit novel LAAO activity. Other procedures, such as preparation of the sequence library and classification, are described in the figure legends; a total of three sequences annotated as the hypothetical protein were obtained by genome mining (Figure

https://doi.org/10.1021/acsomega.2c06334
ACS Omega 2022, 7, 44407−44419

S1). The screened sequences are found in the genome of the *Caulobacter* species, and the estimation of their enzymatic function is difficult because of their locus tag annotating "hypothetical proteins" (Table S1). Here, an ancestral enzyme of the screened sequences was reconstructed according to these representations; the utilized sequences are the minimum number of sequences needed to design an ancestral enzyme by ASR. The reconstructed sequence was named AncLLysO2 (Table S2) because the enzyme exhibited LLysO activity as well as that of the AncLLysO. Here, AncLLysO and AncLLysO2 were reconstructed from distinct sequences that were obtained from different target proteins, sequence libraries, and key residues.[22] The designed enzymes shared low sequence identity (approximately 30%) with each other.

Characterization of Enzymatic Properties of AncLLysO2 by Biochemical Assay. Next, we analyzed the enzymatic properties of AncLLysO2. UV−vis spectra of the purified AncLLysO2 samples indicated that the enzyme has FAD as a cofactor; the characteristic peak of oxidized FAD was observed at the 450 nm region (Figure S2).

Activity toward 20 L-AAs indicated that the enzyme exhibited high specificity toward L-Lys (Figure 1A). Weak activity toward L-Arg (approximately 12% of L-Lys) was also detected (Figure 1A). The thermostability of AncLLysO2 was moderate; the $t_{1/2}$ value was approximately 56 °C (Figure 1B). The optimal pH value of AncLLysO2 was 6.0 (Figure 1C); acetate ions in NaOAc buffer may inhibit the activity of AncLLysO2. The value was slightly shifted to the acidic region compared with AncLLysO.[22] Steady-state kinetic parameters of the AncLLysO2-catalyzed reaction were estimated using three L-AAs (L-Lys, L-Arg, and L-Orn) as substrates, and the plots for their initial velocity are shown in Figure S3. All of the enzymatic reactions were performed at a fixed oxygen concentration. Thus, the kinetic parameters obtained in this study are all apparent values. The parameters indicated that the k_{cat} and k_{cat}/K_m values toward L-Lys were more than one and two orders higher than those of L-Arg and L-Orn, respectively (Table 1).

Compared with other LLysOs, AncLLysO2 exhibited higher specificity toward L-Lys than L-Arg; for the relative k_{cat}/K_m value toward L-Lys in comparison with L-Arg, the value of AncLLysO2 was >5- and 60-fold higher than those of AncLLysO and L-LOX/MOG, respectively (Table 1). The high specificity is expected to be useful in the quantification of L-Lys concentrations in various samples. To confirm this, we performed a quantification assay (Figure 1D). The concentration of L-Lys in the samples with (filled circle) or without plasma (filled square) was estimated by an end-point assay at different concentrations of L-Lys, indicating that AncLLysO2 can apply to quantify L-Lys under conditions containing 0−400 μM L-Lys. Slopes on the plots had almost identical values to each other (Figure 1D) as well as to other L-amino acid quantification enzymes.[22,40,41]

LC-HRMS Analysis of Products Generated by the AncLLysO2 Reaction. Biochemical analysis indicated that AncLLysO2 oxidized L-Lys as expected. The next challenge was to characterize their reaction products. To our knowledge, two bacterial enzymes bearing LLysO activity have been previously identified. Each of the enzymes generates distinct compounds as main products. 5-Amino pentanamide (5-APNM) and 5-amino pentanoic acid (5-APNA) are mainly produced by L-LOX/MOG and AncLLysO, respectively.[21,22] Because of this background, main products of AncLLysO2 may be different from L-LOX/MOG and AncLLysO.

To confirm this point, reaction products of AncLLysO2 were analyzed by LC-HRMS. Referring to the previous study,[22] a total of three reaction conditions were prepared to characterize the products: (a) 10 mM L-Lys; (b) 10 mM L-Lys and 0.5 mg AncLLysO2; and (c) 10 mM L-Lys, 0.5 mg AncLLysO2, and 1000 U catalase (Figure 2). After adding AncLLysO2 and incubating for 24 h, the reaction was stopped by heating the reaction solution. The mixture was centrifuged, and LC-HRMS analysis was performed. The reaction scheme of AncLLysO2 was proposed by referring to the reaction mechanism of L-LOX/MOG and AncLLysO.[19−22] The peak of L-Lys completely disappeared after the addition of AncLLysO2, suggesting that AncLLysO2 reacts with L-Lys as expected (b and c for L-Lys in Figure 2). At the same time, after consumption of L-Lys by AncLLysO2, reaction products were identified: 5-APNA, 5-APNM, and 3,4,5,6-tetrahydropyradine-2-carboxylic acid (TPCA) (b and c in Figure 2). AncLLysO and L-LOX/MOG also generated the products by oxidizing the α-amino group of L-Lys,[21,22] suggesting that AncLLysO2 has L-Lys α-oxidase activity. The amount of produced 5-APNM was less than 10% of L-Lys, as was the case for AncLLysO. The remaining >90% of the L-Lys would be converted to TPCA or 5-APNA (b and c in Figure 2). A high amount of 5-APNM was produced by L-LOX/MOG when the imino acid is kept on the active site and located structurally near to *in situ* H_2O_2.[21] A Small amount of the production of 5-APNM in AncLLysO2 suggested that the imino acid is rapidly released from the active site; small parts of the imino acid may react with *in situ* H_2O_2 coincidentally.

There was a difference between AncLLysO and AncLLysO2 in the production of 5-APNA; under conditions without catalase, 5-APNA was the main product in AncLLysO, whereas the compounds were hardly produced in AncLLysO2 (c in Figure 2).[22] On the contrary, the TPCA, which is generated by self-cyclizing the 2-keto-6-amino hexanoic acid (KH), was the main product in AncLysO2 judging from the concentration of other products, 5-APNA and 5-APNM (b and c in Figure 2); the TPCA concentration could not be quantified because no standard compound is available. In a previous study, Trisrivirat *et al.* reported that 5-APNA is generated by reacting the KH that is produced by hydrolyzing imino acid with *in situ* H_2O_2 at the active site.[21] These results suggest that the intermediates of AncLLysO2 produced, imino acids, would be rapidly released from the active site. After hydrolysis of the imino acids to KH, the self-cyclization occurred in the solvent by the non-enzymatic reaction.

Structure Analysis of AncLLysO2. LC-HRMS analysis indicated that AncLLysO2 catalyzes the oxidation of the α-amino group of L-Lys as the main reaction. The produced imino acids are immediately released from the active site. This suggested that the active site structure or substrate entrance tunnel of AncLLysO2 may be optimized to release the product rapidly to the solvent. The structure of AncLLysO2 would confirm this hypothesis at the molecular level. The crystal structure of the ligand-free form of AncLLysO2 was determined at 1.55 Å resolution (Table 2). The initial phase was determined by the iodide single anomalous dispersion method because no homologous structures were available to perform the molecular replacement. The overall structure of AncLLysO2 is represented in Figure 3A, indicating that the enzyme has the typical fold of the FAO superfamily. This point

https://doi.org/10.1021/acsomega.2c06334
ACS Omega 2022, 7, 44407−44419

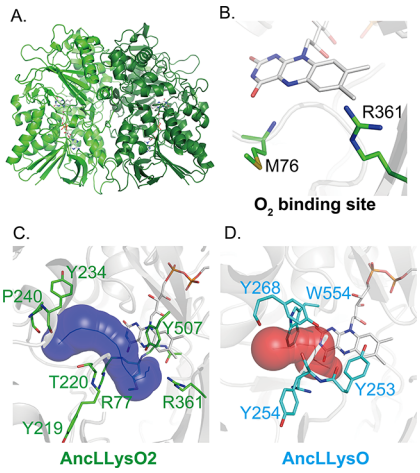

Figure 3. Overall structure of AncLLysO2 (A) and their O_2 binding site (B). The structure indicated that AncLLysO2 is an FAD-dependent oxidase, as expected. Substrate: the entrance pathway of AncLLysO2 (C) and AncLLysO (D). The pathway was estimated by CAVER software. Residues that formed plug loops in AncLLysO2 (Y219 and T220) and AncLLysO (Y253 and Y254) were also represented in the figure by referring to the MSA analysis (Figure S4).

was supported by structural homology analysis with the Dali web server.[42] This analysis demonstrated that all of the top 10 structures, which shared high structural similarity to AncLLysO2, belonged to the FAO superfamily (Table S3).

The enzymatic characteristics of LAAOs, such as substrate recognition, reactivity, and product release, are controlled by the following three regions: the O_2 binding site, substrate entrance pathway, and substrate binding site. Structural comparison of the regions may provide the characteristic reaction mechanism of AncLLysO2 that was revealed by biochemical and LC-HRMS analysis (Figures 1 and 2). First, the oxidation mechanism of $FADH^-$ was predicted from the analysis of the O_2 binding site (Figure 3B), suggesting that the $FADH^-$ is oxidized by the same mechanism as other LAAOs. The O_2 binding site structure is highly conserved with other LAAOs; the sites are formed by a basic residue (R361) and M76 (Figure 3B), which coordinate the O_2 molecule in the correct position to oxidize the $FADH^-$. We performed a structural comparison of the substrate entrance pathway between AncLLysO2 and AncLLysO (Figure 3C,D). Both enzymes had the plug loop on the pathway: GGYY from 251st to 254th residues in AncLLysO and GGYT from 217th to 220th residues in AncLLysO2, respectively (cyan box in Figure S4). The pathway could be assigned to AncLLysO (Figure 3C) and AncLLysO2 (Figure 3D) structures, suggesting that the loop is located in a position to keep the active site in an open state in the ligand-free forms.

Next, crystal structures of the L-Lys- and L-Arg-bound form of AncLLysO2 were determined at 1.6 and 1.4 Å resolutions, respectively. We attempted to obtain the ligand-bound structures of the AncLLysO2(R361A) variant; however, these provided only weakly diffracting crystals (<3.0 Å resolution). Alternatively, ligand-bound structures of AncLLysO2 were determined by soaking the ligand-free crystals in a cryo-reservoir solution containing a high concentration of substrates (100 mM); the oxidation reaction was stopped because O_2 molecules in the cryo-reservoir solution were consumed during the soaking process.[7,43] The polder F_o-F_c

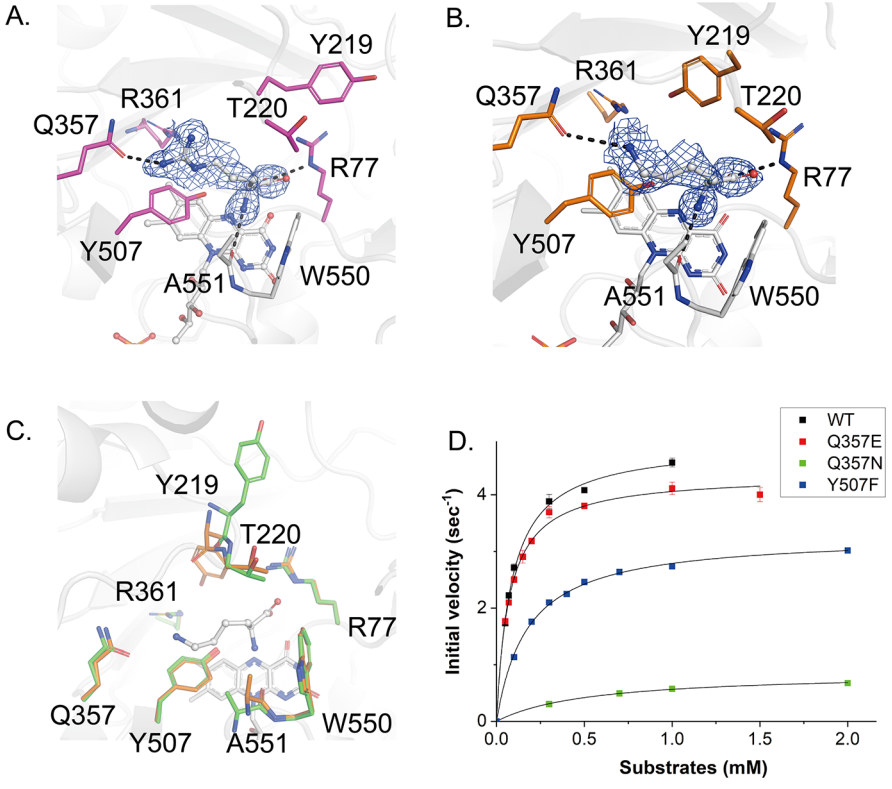

Figure 4. Active site structures of AncLLysO2 bound to L-Arg (A) and L-Lys (B). The polder F_o-F_c map was contoured at 3.0 (A) and 2.5 σ (B). Structure comparison of AncLLysO2 between ligand-free and L-Lys bound forms (C). The structures of ligand-free form and L-Lys bound form are green and orange, respectively. Enzyme kinetic plots of AncLLysO2 and their variants (D). All experiments were performed using six replicates.

https://doi.org/10.1021/acsomega.2c06334
ACS Omega 2022, 7, 44407−44419

map indicated that L-Arg (Figure 4A) and L-Lys (Figure 4B) bind to the active site as expected. The α-amino group of the substrate formed a hydrogen bond with the main chain carbonyl oxygen atom of A551, the carboxyl groups of the substrate formed charge−charge interaction with the guanidinium group of R77, and the ε-amino or guanidinium groups of the substrates (L-Lys or L-Arg) formed the interaction with Q357 (Figure 4A,B), respectively. Three residues, Y219, T220, and Y507, were located near the ε-amino and guanidinium groups of the substrates. The structural change of Y219 is remarkable, and the difference appeared to be induced by binding substrates (Figure 4C). Another notable point is that AncLLysO2 kept an open state after binding the substrates (Figure 4C). This is contrary to AncLLysO and L-LOX/MOG wherein the conformation change of the loop is induced by binding the substrates to plug the active site. Because of the conformation changes observed in L-LOX/MOG and AncLLysO, the products can be trapped in the active site;[21,22] this enables the enzymes to promote the decarboxylation reaction of products—imino acids for L-LOX/MOG and keto acid for AncLLysO—utilizing *in situ* H_2O_2 generated by the oxidation reaction at the active site. On the other hand for AncLLysO2, the active site is exposed to the solvent, and the enzyme can release the product immediately after the reaction. As confirmed in LC-HRMS analysis, this would repress the decarboxylation reaction in AncLLysO2 (Figure 2).

To predict the functional roles of active site residues, we analyzed the enzyme kinetics of AncLLysO2 variants, which were expressed in soluble form (Figure 4D). A mutation at the residues forming hydrogen bonds with the substrate drastically reduced its activity. The activity of R77A was too low to estimate the kinetic parameters; the mutation made it difficult for AncLLysO2 to form hydrogen bonds with the carboxyl group of the substrate. For the Q357N variant, which shortens the side chain length at the 357th position, the k_{cat}/K_m value was one order lower than the original form. On the other hand, the value was comparable to the original one for the Q357E mutant, which has an identical side chain length but has a negative charge because of the mutation (Table 3). These data support that Q357 is important to form interactions with the ε-amino group of L-Lys, as expected from the crystal structure (Figure 4B). For the mutations of the residues located near the substrate, the reduction of the parameters was remarkable when the aromatic residues were mutated to Ala. The k_{cat}/K_m values of Y219F and Y507F were approximately 1.3- and 3-fold lower than that of the native form (Table 3), respectively. In contrast, the Y219A variant was inactivated despite the fact that the residue forms no direct interaction with the substrate (Figure 4B and Table 3). The activity of Y219A variant toward L-Arg was >one-order lower than that of L-Lys.

Table 3. Enzyme Kinetic Parameters of AncLLysO2 Variants toward L-Lys[a]

sample name	k_{cat} (s^{-1})	K_m (mM)	k_{cat}/K_m (s^{-1} mM^{-1})
WT	4.91 ± 0.08	0.086 ± 0.005	57.4
	O_2 Recognition Site		
R361A	N.D.	N.D.	N.D.
	Substrate Recognition Site		
R77A	N.D.	N.D.	N.D.
Y219A	N.D.	N.D.	N.D.
Y219F	2.00 ± 0.05	0.044 ± 0.004	45.5
Q357E	4.35 ± 0.07	0.072 ± 0.004	60
Q357N	0.86 ± 0.02	0.53 ± 0.03	1.6
Y507F	3.28 ± 0.04	0.18 ± 0.007	18.5

[a]The measurement of enzyme kinetic parameters was performed independently in six times ($N = 6$). ND means "not determined" because of low activity.

Taken together, we revealed the substrate recognition mechanism of AncLLysO2 by combinational analysis of ligand-binding structures and enzyme kinetics analysis of the variants. In this study, we focused on revealing the substrate recognition mechanism of AncLLysO2 at the molecular level. The next challenge is to reveal the mechanism of substrate entrance of AncLLysO2.

Molecular Dynamics Simulation of AncLLysO2. Structural analysis of the ligand-bound form of AncLLysO2 indicated that the conformational change of Y219 is remarkable compared with other active site residues. Inactivation of the Y219A variant, and not for the Y219F variant, was confirmed by enzyme kinetic analysis, suggesting that the side chain of Y219, especially for an aromatic group, is important for an activity to be demonstrated. To predict the function of Y219, we attempted to compare the dynamics of AncLLysO2 and the Y219A variant in solution by using MD simulations. A 200 ns simulation was performed for each system, and the results are shown in Figure 5. Plots for the root-mean-square deviation (RMSD) value for Cα atoms of AncLLysO2 and the Y219A variant indicated that the simulation was correctly performed; the values were equilibrated at 1.4 Å (Figure 5A). Root-mean-square fluctuation (RMSF) values for Cα atoms were calculated to evaluate flexibility change caused by the mutation. The difference of RMSF values (ΔRMSF), calculated by subtracting the values of AncLLysO2 from the values of the Y219A variant, is shown in Figure 5B, indicating that the Y219A mutation increased the flexibility, and the average ΔRMSF value was 0.06 Å.

The analysis of RMSD and ΔRMSF values suggested that the Y219A mutation would affect flexibility but not the overall structure of AncLLysO2. Next, we attempted to reveal how the mutation affects the dynamics of the substrate L-Lys. The time-dependent change of the distance between N5(FAD) and CA of the bound L-Lys substrate atoms is shown in Figure 5C, indicating that the distance was changed in the Y219A variant (red line in Figure 5C) compared with AncLLysO2 (black line in Figure 5C). Structural comparison between AncLLysO2 (Figure 5D) and the Y219A variant (Figure 5E) at the final state of the MD simulation suggested that the L-Lys substrate in the Y219A variant can be moved to the cavity during the simulation, and this weakens the interaction between L-Lys and AncLLysO2(Y219A). The MM-GB/SA value for the Y219A variant (−22.48 kcal/mol) was greater than 4 kcal/mol less negative than AncLLysO2 (−26.86 kcal/mol). Taken together, Y219 is important to position the L-Lys substrate correctly in order for the reaction to proceed.

Structural and Functional Comparison between AncLLysO2 and Other LLysOs. Biochemical, structural, and computational analysis of AncLLysO2 indicated that the enzyme is a less promiscuous L-Lys α-oxidase having no pro-sequence; LAAO activity is often toxic for living organisms, so to reduce the activity under *in vivo* conditions, several of the LAAOs hinder the substrate entrance pathway by the pro-sequence.[44,45] The properties were different from other LLysOs; catalytic promiscuity (oxidase and mono-oxygenase

https://doi.org/10.1021/acsomega.2c06334
ACS Omega 2022, 7, 44407−44419

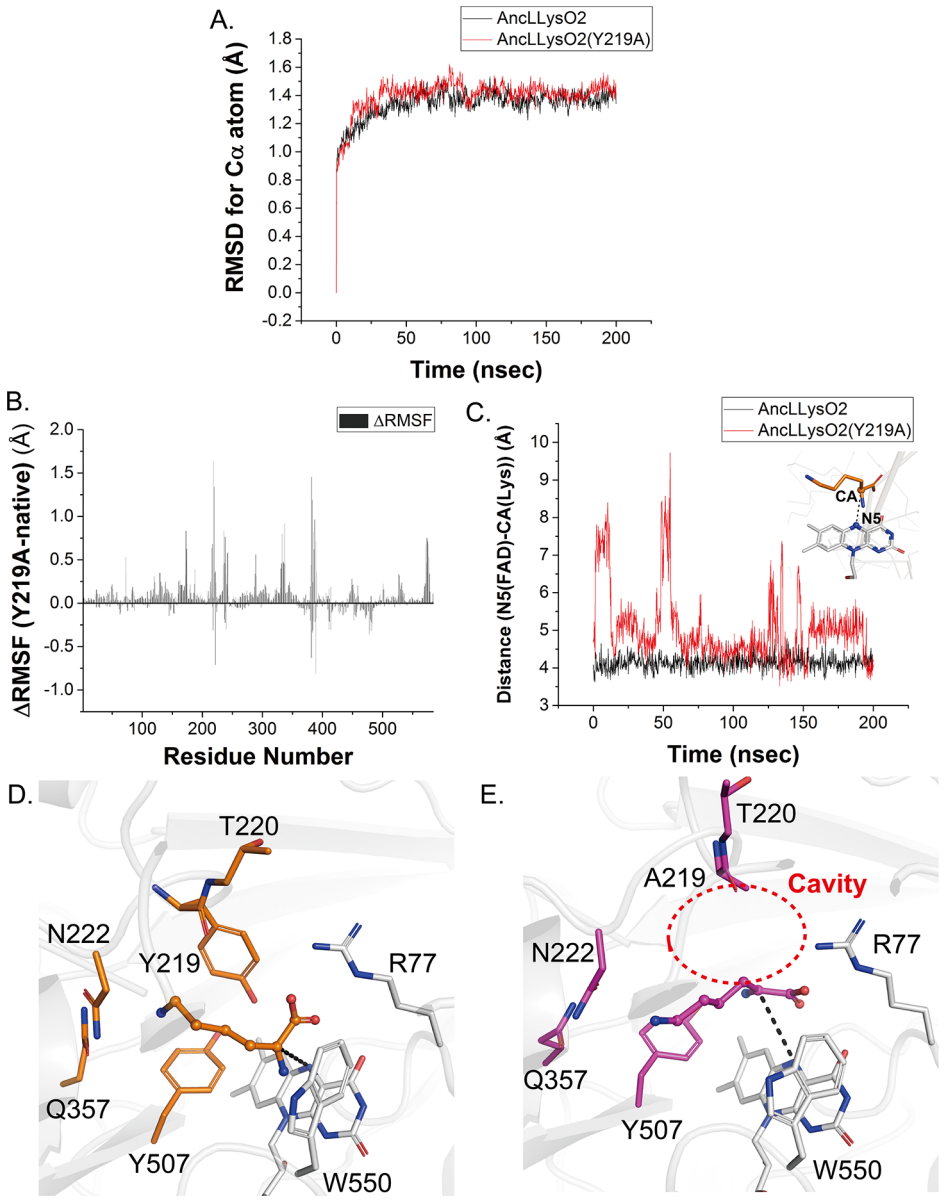

Figure 5. Time-dependent change of the RMSD value for Cα atoms of AncLLysO2 (black) and AncLLysO2(Y219A) variant (red) (A). Plots of ΔRMSF values for Cα atoms of each residue of AncLLysO2 (B). The values were calculated by subtracting the values of AncLLysO2 from the values of AncLLysO2(Y219A). Time-dependent change of distance between N5(FAD) and CA of the bound L-Lys substrate atoms of AncLLysO2 (black) and the Y219A variant (red) (C). Active site structure comparison of AncLLysO2 (D) and the Y219A variant (E) at the final state (200 ns) of the MD simulation. The structures of the AncLLysO2 and Y219A variants are orange and magenta, respectively.

activity) was confirmed in AncLLysO and L-LOX/MOG, and L-Lys α-oxidase from *Trichoderma viride* (TvLysO) matured by cleaving the pro-sequence.[46] Sequence identity among the enzymes was <32% (Table S4), suggesting that the enzymes have unique substrate recognition mechanisms.

To confirm this point, a structural comparison at the active site was performed for the four LLysOs. The interaction that formed between the ε-amino group of substrate L-Lys and active site residues differed between AncLLysO2 and the other two LLysOs, L-LOX/MOG and TvLysO (Figure 6); compared with Q357 in AncLLysO2, D238 (L-LOX/MOG) and D289 (TvLysO) are placed at different positions in the structure and sequence (Figure 6 and red box in Figure S4). Although the substrate recognition mechanism is highly similar between AncLLysO2 and AncLLysO (Figure 6), conformational change in the plug loop differs between the two. In AncLLysO2, the active site has a more open form during the reaction because there is no conformational change in the plug loop; this enables AncLLysO2 to release the product, imino acid, rapidly to the solvent. On the other hand for AncLLysO, the active site is closed during the reaction because of the conformational change in the plug loop.[22] KH would be kept on the active site, and *in situ* H_2O_2 can react with KH to produce 5-APNA.[22] Because of the difference in the substrate recognition mechanism, the KH may be remotely located from the FAD cofactor in AncLLysO, producing more 5-APNA than 5-APNM, as is the case for the reaction of L-Orn in L-LOX/MOG.[21]

Proposed Reaction Mechanism of AncLLysO2. Summarizing the results, the proposed reaction mechanism of AncLLysO2 is shown in Figure 7. The active site of AncLLysO2 was formed by six residues: R77, Y219, Q357,

https://doi.org/10.1021/acsomega.2c06334
ACS Omega 2022, 7, 44407−44419

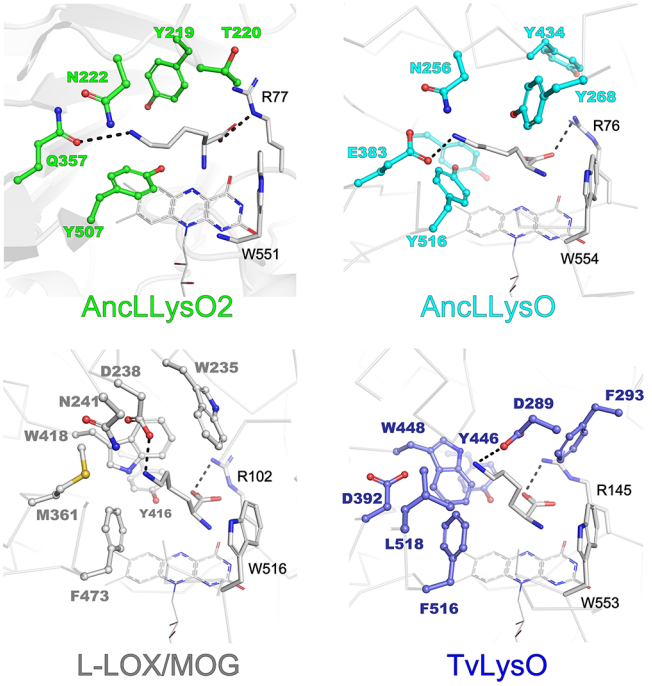

Figure 6. Structural comparison at the active site among four LLysOs. Structures of AncLLysO2, AncLLysO (PDB ID: 7EII), L-LOX/MOG (PDB ID: 5YB6), and TvLysO (PDB ID: 7D4E) are colored by green, cyan, gray, and deep blue, respectively.

Y507, W550, and A551. There is enough space to bind substrates in the ligand-free form of AncLLysO2, and only a conformational change of Y219 is induced by the binding of L-Lys (upper right of Figure 7). This differs from AncLLysO in that the cavity of the active site is occupied by side chain groups of Y254 in the ligand-free form.[22] L-Lys would coordinate with AncLLysO2 to form interactions with R77, Q357, and A551. As with other LAAOs, oxidation of L-Lys would progress as shown in the scheme (lower right of Figure 7). In the process, there is a possibility that the activated H_2O molecule, which is not confirmed in AncLLysO2 structures, deprotonates the α-amino group of the substrate. The resulting imino acid is rapidly released into the solvent, and simultaneously, a structural change of Y219 is induced (lower left of Figure 7). As shown in Figure 2, the released imino acid is hydrolyzed to keto acid, and self-cyclization progresses continuously to generate TPCA by the non-enzymatic reaction. The $FADH^-$ is oxidized by the O_2 molecule, which is coordinated to R361, and H_2O_2 is released into the solvent (upper left of Figure 7).

CONCLUSIONS

In this study, we designed synthetic proteins bearing LLysO activity, named AncLLysO2, from functionally uncharacterized sequences in the FAO superfamily using genome mining and ASR. AncLLysO2 exhibited strong oxidase activity and high specificity toward L-Lys than other LLysOs. This enables the enzyme to be applied in quantifying the L-Lys concentration in

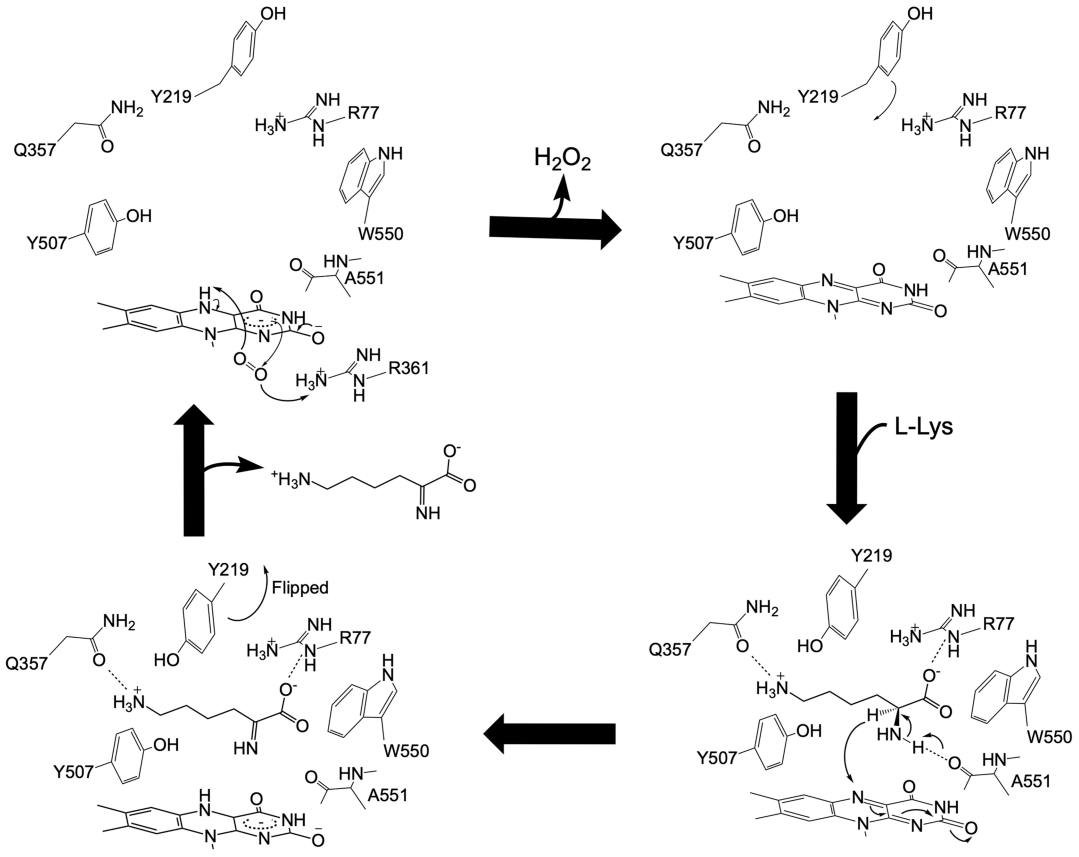

Figure 7. Proposed reaction scheme of AncLLysO2. In this scheme, ligand-free, ligand-binding, and product-binding forms are represented in the upper right, lower right, and lower left positions, respectively. After completion of product release, the FADH was oxidized by the O_2 molecule, which is coordinated to R361 (upper left).

https://doi.org/10.1021/acsomega.2c06334
ACS Omega 2022, 7, 44407−44419

various samples. The unique enzymatic properties of AncLLysO2 are a result of conformational change in the plug loop. The active site of AncLLysO2 was kept on an open state during the reaction despite the fact that the conformation change was induced by the binding of the substrates; this was different from AncLLysO and L-LOX/MOG wherein the conformation of the loop was changed to a closed state to trap the products at the active site.[21,22] Conformation changes of the loop observed in AncLLysO2 enable it to easily release the products into the solvent. Summarizing the biochemical, structural, and computational analysis of AncLLysO2 and its variants, we proposed the reaction mechanism. Currently, 15 hypothetical proteins from *Caulobacter* species that shared >80% sequence identity with AncLLysO2 have been registered in the sequence database (Table S6). Active site structures of the hypothetical proteins are identical to those of AncLLysO2, suggesting that the proteins would exhibit LLysO activity as well as AncLLysO2.

FUNDING

This work was supported by JSPS KAKENHI grant numbers 18 K14391 and 21 K05395 and by JST, PRESTO grant number JPMJPR20AB.

AUTHOR CONTRIBUTION

S.N. designed AncLLysO2. C.I. and Y.K. performed the biochemical assays for AncLLysO2 and their variants. T.M. determined X-ray crystal structures of AncLLysO2. Y.Y. and Y.S. performed molecular dynamics simulations of AncLLysO2 and the Y219A variant. F.H. performed the LC-HRMS analysis to assign the products of AncLLysO2. S.N., S.I., and Y.S. managed the research. S.N. wrote the manuscript. All authors contributed to the article and approved the submitted version.

ASSOCIATED CONTENT

Supporting Information

The Supporting Information is available free of charge at https://pubs.acs.org/doi/10.1021/acsomega.2c06334.

Schematic view for the design of AncLLysO2 (Figure S1), UV−vis spectra of the purified AncLLysO2 (Figure S2), steady-state enzyme kinetic plots of AncLLysO2 (Figure S3), multiple sequence alignment of four LLysOs (Figure S4), three hypothetical protein sequences that are utilized to design AncLLysO2 (Table S1), protein and DNA sequences of AncLLysO2 (Table S2), top 10 structures that have structural similarity to AncLLysO2 (Table S3), sequence identity between the functionally assigned LLysOs belonging to the FAO superfamily (Table S4), and primer list to prepare site-directed variants of AncLLysO2 (Table S5) (PDF)

AUTHOR INFORMATION

Corresponding Authors

Yasuteru Shigeta − *Center for Computational Sciences, University of Tsukuba, Tsukuba, Ibaraki 305-8577, Japan;* orcid.org/0000-0002-3219-6007; Email: shigeta@ccs.tsukuba.ac.jp

Sohei Ito − *Graduate Division of Nutritional and Environmental Sciences, University of Shizuoka, Shizuoka 422-8526, Japan;* orcid.org/0000-0002-9937-3100; Phone: +81-54-264-5578; Email: itosohei@u-shizuoka-ken.ac.jp

Shogo Nakano − *Graduate Division of Nutritional and Environmental Sciences, University of Shizuoka, Shizuoka 422-8526, Japan; PREST, Japan Science and Technology Agency, Saitama 332-0012, Japan;* orcid.org/0000-0002-6614-7158; Phone: +81-54-264-5538; Email: snakano@u-shizuoka-ken.ac.jp

Authors

Tomoharu Motoyama − *Graduate Division of Nutritional and Environmental Sciences, University of Shizuoka, Shizuoka 422-8526, Japan*

Yuta Yamamoto − *Department of Physics, Graduate School of Pure and Applied Sciences, University of Tsukuba, Tsukuba, Ibaraki 305-8577, Japan*

Chiharu Ishida − *Graduate Division of Nutritional and Environmental Sciences, University of Shizuoka, Shizuoka 422-8526, Japan*

Fumihito Hasebe − *Department of Bioscience, Fukui Prefectural University, Fukui 910-1195, Japan;* orcid.org/0000-0002-1097-3813

Yui Kawamura − *Graduate Division of Nutritional and Environmental Sciences, University of Shizuoka, Shizuoka 422-8526, Japan*

Complete contact information is available at: https://pubs.acs.org/10.1021/acsomega.2c06334

Author Contributions

#T.M., Y.Y., and C.I. contributed equally to this work.

Notes

The authors declare no competing financial interest.

ACKNOWLEDGMENTS

X-ray data were collected at the synchrotron facilities of the Photon Factory using beamline BL-5A (2018G006 and 2020G007). The authors are grateful to the beamline staff for their assistance with the experiments performed at the Photon Factory.

REFERENCES

(1) Facchini, P. J.; Huber-Allanach, K. L.; Tari, L. W. Plant aromatic L-amino acid decarboxylases: evolution, biochemistry, regulation, and metabolic engineering applications. *Phytochemistry* **2000**, *54*, 121−138.

(2) Wu, G. Amino acids: metabolism, functions, and nutrition. *Amino Acids* **2009**, *37*, 1−17.

(3) Pollegioni, L.; Motta, P.; Molla, G. L-amino acid oxidase as biocatalyst: a dream too far? *Appl. Microbiol. Biotechnol.* **2013**, *97*, 9323−9341.

(4) Hossain, G. S.; Li, J.; Shin, H. D.; Du, G.; Liu, L.; Chen, J. L-Amino acid oxidases from microbial sources: types, properties, functions, and applications. *Appl. Microbiol. Biotechnol.* **2014**, *98*, 1507−1515.

(5) Ehara, T.; Kitajima, S.; Kanzawa, N.; Tamiya, T.; Tsuchiya, T. Antimicrobial action of achacin is mediated by L-amino acid oxidase activity. *FEBS Lett.* **2002**, *531*, 509−512.

(6) Ishida, C.; Miyata, R.; Hasebe, F.; Miyata, A.; Kumazawa, S.; Ito, S.; Nakano, S. Reconstruction of Hyper-Thermostable Ancestral L-Amino Acid Oxidase to Perform Deracemization to D-Amino Acids. *ChemCatChem* **2021**, *13*, 5228−5235.

(7) Nakano, S.; Kozuka, K.; Minamino, Y.; Karasuda, H.; Hasebe, F.; Ito, S. Ancestral L-amino acid oxidases for deracemization and stereoinversion of amino acids. *Commun. Chem.* **2020**, *3*, 181.

(8) Schnepel, C.; Kemker, I.; Sewald, N. One-Pot Synthesis of d-Halotryptophans by Dynamic Stereoinversion Using a Specific l-Amino Acid Oxidase. *ACS Catal.* **2019**, *9*, 1149−1158.
(9) Alexandre, F.-R.; Pantaleone, D. P.; Taylor, P. P.; Fotheringham, I. G.; Ager, D. J.; Turner, N. J. Amine−boranes: effective reducing agents for the deracemisation of dl-amino acids using l-amino acid oxidase from Proteus myxofaciens. *Tetrahedron Lett.* **2002**, *43*, 707−710.
(10) Tararina, M. A.; Allen, K. N. Bioinformatic Analysis of the Flavin-Dependent Amine Oxidase Superfamily: Adaptations for Substrate Specificity and Catalytic Diversity. *J. Mol. Biol.* **2020**, *432*, 3269−3288.
(11) Robinson, S. L.; Piel, J.; Sunagawa, S. A roadmap for metagenomic enzyme discovery. *Nat. Prod. Rep.* **2021**, *38*, 1994−2023.
(12) Merkl, R.; Sterner, R. Ancestral protein reconstruction: techniques and applications. *Biol. Chem.* **2016**, *397*, 1−21.
(13) Gumulya, Y.; Gillam, E. M. J. Exploring the past and the future of protein evolution with ancestral sequence reconstruction: the 'retro' approach to protein engineering. *Biochem. J.* **2017**, *474*, 1−19.
(14) Gomez-Fernandez, B. J.; Risso, V. A.; Rueda, A.; Sanchez-Ruiz, J. M.; Alcalde, M. Correction for Gomez-Fernandez et al., "Ancestral Resurrection and Directed Evolution of Fungal Mesozoic Laccases". *Appl. Environ. Microbiol.* **2020**, *86*, No. e01732-20.
(15) Gumulya, Y.; Baek, J.-M.; Wun, S.-J.; Thomson, R. E. S.; Harris, K. L.; Hunter, D. J. B.; Behrendorff, J. B. Y. H.; Kulig, J.; Zheng, S.; Wu, X.; Wu, B.; Stok, J. E.; De Voss, J. J.; Schenk, G.; Jurva, U.; Andersson, S.; Isin, E. M.; Bodén, M.; Guddat, L.; Gillam, E. M. J. Engineering highly functional thermostable proteins using ancestral sequence reconstruction. *Nat. Catal.* **2018**, *1*, 878−888.
(16) Kido, K.; Yamanaka, S.; Nakano, S.; Motani, K.; Shinohara, S.; Nozawa, A.; Kosako, H.; Ito, S.; Sawasaki, T. AirID, a novel proximity biotinylation enzyme, for analysis of protein-protein interactions. *Elife* **2020**, *9*, No. e54983.
(17) Nicoll, C. R.; Bailleul, G.; Fiorentini, F.; Mascotti, M. L.; Fraaije, M. W.; Mattevi, A. Ancestral-sequence reconstruction unveils the structural basis of function in mammalian FMOs. *Nat. Struct. Mol. Biol.* **2020**, *27*, 14−24.
(18) Takagi, H.; Kozuka, K.; Mimura, K.; Nakano, S.; Ito, S. Design of a Full-Consensus Glutamate Decarboxylase and Its Application to GABA Biosynthesis. *ChemBioChem* **2022**, *23*, No. e202100447.
(19) Matsui, D.; Im, D. H.; Sugawara, A.; Fukuta, Y.; Fushinobu, S.; Isobe, K.; Asano, Y. Mutational and crystallographic analysis of l-amino acid oxidase/monooxygenase from Pseudomonas sp. AIU 813: Interconversion between oxidase and monooxygenase activities. *FEBS Open Bio* **2014**, *4*, 220−228.
(20) Im, D.; Matsui, D.; Arakawa, T.; Isobe, K.; Asano, Y.; Fushinobu, S. Ligand complex structures of l-amino acid oxidase/monooxygenase from Pseudomonas sp. AIU 813 and its conformational change. *FEBS Open Bio* **2018**, *8*, 314−324.
(21) Trisrivirat, D.; Lawan, N.; Chenprakhon, P.; Matsui, D.; Asano, Y.; Chaiyen, P. Mechanistic insights into the dual activities of the single active site of l-lysine oxidase/monooxygenase from Pseudomonas sp. AIU 813. *J. Biol. Chem.* **2020**, *295*, 11246−11261.
(22) Sugiura, S.; Nakano, S.; Niwa, M.; Hasebe, F.; Matsui, D.; Ito, S. Catalytic mechanism of ancestral L-lysine oxidase assigned by sequence data mining. *J. Biol. Chem.* **2021**, *297*, No. 101043.
(23) Yamada, K. D.; Tomii, K.; Katoh, K. Application of the MAFFT sequence alignment program to large data-reexamination of the usefulness of chained guide trees. *Bioinformatics* **2016**, *32*, 3246−3251.
(24) Guindon, S.; Dufayard, J. F.; Lefort, V.; Anisimova, M.; Hordijk, W.; Gascuel, O. New algorithms and methods to estimate maximum-likelihood phylogenies: assessing the performance of PhyML 3.0. *Syst. Biol.* **2010**, *59*, 307−321.
(25) Yang, Z. PAML 4: phylogenetic analysis by maximum likelihood. *Mol. Biol. Evol.* **2007**, *24*, 1586−1591.
(26) Kabsch, W. Xds. *Acta Crystallogr., Sect. D: Biol. Crystallogr.* **2010**, *66*, 125−132.
(27) Evans, P. Scaling and assessment of data quality. *Acta Crystallogr., Sect. D: Biol. Crystallogr.* **2006**, *62*, 72−82.
(28) Adams, P. D.; Afonine, P. V.; Bunkoczi, G.; Chen, V. B.; Davis, I. W.; Echols, N.; Headd, J. J.; Hung, L. W.; Kapral, G. J.; Grosse-Kunstleve, R. W.; McCoy, A. J.; Moriarty, N. W.; Oeffner, R.; Read, R. J.; Richardson, D. C.; Richardson, J. S.; Terwilliger, T. C.; Zwart, P. H. PHENIX: a comprehensive Python-based system for macromolecular structure solution. *Acta Crystallogr., Sect. D: Biol. Crystallogr.* **2010**, *66*, 213−221.
(29) Emsley, P.; Lohkamp, B.; Scott, W. G.; Cowtan, K. Features and development of Coot. *Acta Crystallogr., Sect. D: Biol. Crystallogr.* **2010**, *66*, 486−501.
(30) Vagin, A.; Teplyakov, A. Molecular replacement with MOLREP. *Acta Crystallogr., Sect. D: Biol. Crystallogr.* **2010**, *66*, 22−25.
(31) Murshudov, G. N.; Skubák, P.; Lebedev, A. A.; Pannu, N. S.; Steiner, R. A.; Nicholls, R. A.; Winn, M. D.; Long, F.; Vagin, A. A. REFMAC5 for the refinement of macromolecular crystal structures. *Acta Crystallogr., Sect. D: Biol. Crystallogr.* **2011**, *67*, 355−367.
(32) Delano, W. L. *The PyMOL molecular graphics system*; 2002, Delano Scientific, S. C., CA, Ed.; CiNii.
(33) Olsson, M. H. M.; Søndergaard, C. R.; Rostkowski, M.; Jensen, J. H. PROPKA3: Consistent Treatment of Internal and Surface Residues in Empirical pKa Predictions. *J. Chem. Theory Comput.* **2011**, *7*, 525−537.
(34) Abraham, M. J.; Van Der Spoel, D.; Lindahl, E.; Hess, B. *The GROMACS development team GROMACS User Manual version* 2019.
(35) Maier, J. A.; Martinez, C.; Kasavajhala, K.; Wickstrom, L.; Hauser, K. E.; Simmerling, C. ff14SB: Improving the Accuracy of Protein Side Chain and Backbone Parameters from ff99SB. *J. Chem. Theory Comput.* **2015**, *11*, 3696−3713.
(36) Antony, J.; Medvedev, D. M.; Stuchebrukhov, A. A. Theoretical Study of Electron Transfer between the Photolyase Catalytic Cofactor $FADH^{-}$ and DNA Thymine Dimer. *J. Am. Chem. Soc.* **2000**, *122*, 1057−1065.
(37) Miller, B. R., III; McGee, T. D., Jr.; Swails, J. M.; Homeyer, N.; Gohlke, H.; Roitberg, A. E. MMPBSA.py: An Efficient Program for End-State Free Energy Calculations. *J. Chem. Theory Comput.* **2012**, *8*, 3314−3321.
(38) Case, D. A.; Betz, R. M.; Cerutti, D. S.; Cheatham, T. E., III; Darden, T. A.; Duke, R. E.; Giese, T. J.; Gohlke, H.; Goetz, A. W.; Homeyer, N.; Izadi, S.; Janowski, P.; Kaus, J.; Kovalenko, A.; Lee, T. S.; LeGrand, S.; Li, P.; Lin, C.; Luchko, T.; Luo, R.; Madej, B.; Mermelstein, D.; Merz, K. M.; Monard, G.; Nguyen, H.; Nguyen, H. T.; Omelyan, I.; Onufriev, A.; Roe, D. R.; Roitberg, A.; Sagui, C.; Simmerling, C. L.; Botello-Smith, W. M.; Swails, J.; Walker, R. C.; Wang, J.; Wolf, R. M.; Wu, X.; Xiao, L.; Kollman, P. A. *AMBER 16*, University of California, San Francisco, 2016.
(39) Nakano, S.; Minamino, Y.; Hasebe, F.; Ito, S. Deracemization and Stereoinversion to Aromatic d-Amino Acid Derivatives with Ancestral l-Amino Acid Oxidase. *ACS Catal.* **2019**, *9*, 10152−10158.
(40) Matsui, D.; Terai, A.; Asano, Y. L-Arginine oxidase from Pseudomonas sp. TPU 7192: Characterization, gene cloning, heterologous expression, and application to L-arginine determination. *Enzyme Microb. Technol.* **2016**, *82*, 151−157.
(41) Nakano, S.; Niwa, M.; Asano, Y.; Ito, S. Following the Evolutionary Track of a Highly Specific l-Arginine Oxidase by Reconstruction and Biochemical Analysis of Ancestral and Native Enzymes. *Appl. Environ. Microbiol.* **2019**, *85*, e00459−e00419.
(42) Holm, L.; Rosenström, P. Dali server: conservation mapping in 3D. *Nucleic Acids Res.* **2010**, *38*, W545−W549.
(43) Yasukawa, K.; Nakano, S.; Asano, Y. Tailoring D-amino acid oxidase from the pig kidney to R-stereoselective amine oxidase and its use in the deracemization of alpha-methylbenzylamine. *Angew. Chem., Int. Ed. Engl.* **2014**, *53*, 4428−4431.
(44) Ida, K.; Kurabayashi, M.; Suguro, M.; Hiruma, Y.; Hikima, T.; Yamomoto, M.; Suzuki, H. Structural basis of proteolytic activation of L-phenylalanine oxidase from Pseudomonas sp. P-501. *J. Biol. Chem.* **2008**, *283*, 16584−16590.

https://doi.org/10.1021/acsomega.2c06334
ACS Omega 2022, 7, 44407−44419

(45) Amano, M.; Mizuguchi, H.; Sano, T.; Kondo, H.; Shinyashiki, K.; Inagaki, J.; Tamura, T.; Kawaguchi, T.; Kusakabe, H.; Imada, K.; Inagaki, K. Recombinant expression, molecular characterization and crystal structure of antitumor enzyme, L-lysine α-oxidase from Trichoderma viride. *J. Biochem.* **2015**, *157*, 549−559.
(46) Kitagawa, M.; Ito, N.; Matsumoto, Y.; Saito, M.; Tamura, T.; Kusakabe, H.; Inagaki, K.; Imada, K. Structural basis of enzyme activity regulation by the propeptide of l-lysine α-oxidase precursor from Trichoderma viride. *J. Struct. Biol.: X* **2021**, *5*, No. 100044.

https://doi.org/10.1021/acsomega.2c06334
ACS Omega 2022, 7, 44407−44419